Water Air Soil Pollut (2012) 223:3281–3293
DOI 10.1007/s11270-012-1109-5

Removal of Bisphenol A and 17β-Estradiol by Single-Walled Carbon Nanotubes in Aqueous Solution: Adsorption and Molecular Modeling

Qammer Zaib · Iftheker A. Khan · Navid B. Saleh · Joseph R. V. Flora · Yong-Gyun Park · Yeomin Yoon

Received: 13 October 2011 / Accepted: 9 February 2012 / Published online: 1 May 2012

Abstract Single-walled carbon nanotubes, both before (SWNTs) and after treatment (t-SWNTs) with acidified ammonium persulfate, were successfully used to adsorb bisphenol A (BPA) and 17β-estradiol (E2) from aqueous systems. The surface characteristics of the SWNTs and t-SWNTs were analyzed by measuring their surface charge and by imaging their morphological properties through transmission electron microscopy. The extent of defects on the SWNT scaffold generated through acid etching was analyzed by Raman spectroscopy. A total of 19.4, 15.4, and 14.3 mg/g of BPA was adsorbed on SWNTs, while a total of 8.0, 6.4, and 5.1 mg/g was adsorbed on t-SWNTs with a 72-h contact time at 280, 295, and 315 K, respectively. A significantly high fraction of E2 (27.2 mg/g) was absorbed by both SWNTs and t-SWNTs, as compared to BPA. The adsorption kinetics was analyzed using a pseudo-second-order model. Sorption experiments showed that t-SWNTs adsorbed less than half as much BPA as SWNTs, but their E2 adsorption was similar. The sorption mechanism was investigated by performing molecular-level calculations. Adsorption energies calculated using density functional theory show preferential sorption of E2 to SWNTs and graphene (−26.2 kcal/mol on SWNT and −34.1 kcal/mol on graphene) compared to BPA (−17.1 kcal/mol on SWNT and −22.5 kcal/mol on graphene), which were consistent with the experimental findings. Thus, ab initio calculations can mechanistically explain the adsorption differences of BPA and E2 on SWNTs.

Keywords Bisphenol A · 17β-Estradiol · Single-walled carbon nanotubes · Adsorption kinetics · Adsorption energy · Density functional theory

Electronic supplementary material The online version of this article (doi:10.1007/s11270-012-1109-5) contains supplementary material, which is available to authorized users.

Q. Zaib · I. A. Khan · N. B. Saleh · J. R. V. Flora · Y. Yoon (✉)
Department of Civil and Environmental Engineering, University of South Carolina, Columbia, SC 29208, USA
e-mail: yoony@cec.sc.edu

Y.-G. Park
Environmental and Energy Research Team, GS E&C Research Institute, 417-1 Deokseong-ri Ydong-myeon, Cheoin-gu Yongin-si, Gyeonggi-do 449-831, South Korea

1 Introduction

Endocrine-disrupting compounds (EDCs) have been found at parts-per-trillion (ng/L) levels in drinking water, surface water, groundwater, and/or wastewater environments (Kolpin et al. 2002; Yoon et al. 2010). EDCs can mimic natural hormones in the endocrine systems of animals, and thus adversely impact ecosystems and human health by disrupting growth, development, and reproduction (Huang and Weber 2005).

As they remain biologically effective at very low concentrations, it is economically unfeasible to remove them by conventional physicochemical and biological treatment processes (Snyder et al. 2003). Also, poor removal of these compounds was observed when they were sorbed onto minerals, activated carbons, colloids derived from active sludge, and hybrid particles (Pan et al. 2008). Among the EDCs, bisphenol A (BPA) and 17β-estradiol (E2) are the most widely occurring and well-studied (Bautista-Toledo et al. 2005; Fan et al. 2007; Huang and Weber 2005; Kuo 2009; Pan et al. 2008). BPA is a phenolic EDC used as a monomer in the production of polycarbonate plastics, epoxy resins, and flame retardants (Liu et al. 2009), and is able to leach out under normal use conditions (Goodson et al. 2004). E2 is a natural female hormone excreted by humans, livestock, and wildlife (Fan et al. 2007). Thus, BPA and E2 are frequently found in sewage and surface waters (Laganà et al. 2004), which raises concerns about their interaction with suspended colloids, including nanomaterials.

Carbonaceous nanomaterials are the most-studied emerging nanomaterials in recent years (Baughman et al. 2002; Furtado et al. 2004; Mauter and Elimelech 2008; Pan et al. 2010; Pan and Xing 2010). They can be classified as nanodiamonds, fullerenes, carbon onions, graphene, multiwalled carbon nanotubes (MWNTs), and single-walled carbon nanotubes (SWNTs; Mauter and Elimelech 2008). Among these, SWNTs, MWNTs, and fullerenes have shown high adsorption capacities for polyaromatic hydrocarbons (Yang et al. 2006), natural organic matter (Su and Lu 2007), herbicides (Pyrzynska et al. 2007), fluoride (Li et al. 2003), and heavy metals (Li et al. 2002). SWNTs are of particular importance due to their unique properties, which have inspired a vast range of applications including catalytic supports, hydrogen storage elements, nanomechanical devices, mechanical reinforcements, sensors, infrared emitters, field emission sources, scanning probes, conductive films, transistors, interconnects, and logic gates (Baughman et al. 2002; Hersam 2008). This enhanced usage has increased their production, and thereby the likelihood of their release into water bodies, and water and wastewater treatment facilities (Plata et al. 2008). Several studies have reported the use of SWNTs as an adsorbent for EDCs (Pan et al. 2010; Wang et al. 2010), describing their adsorption and hysteresis (Pan et al. 2008), the effect of the concentration on their kinetics (Pan et al. 2010), and their competitive and complementary adsorption (Pan and Xing 2010).

SWNTs are reported to interact with organic chemicals (Ferguson et al. 2008) including EDCs (Pan et al. 2008; Pan et al. 2010; Pan and Xing 2010). Such interaction changes the bioavailability, mobility, and environmental risk of these chemicals (Ferguson et al. 2008; Yang and Xing 2007). The uniform surface and well-defined structure of SWNTs qualify them for mechanistic studies. However, adsorption studies of EDCs to-date (Bautista-Toledo et al. 2005; Huang and Weber 2005; Kuo 2009; Liu et al. 2009; Pan and Xing 2010) cannot provide with in-depth mechanistic understanding of the sorption mechanisms. The adsorption mechanism can be better understood by analyzing the kinetic behavior (Gonzo and Gonzo 2005; Ho et al. 2000; Liu et al. 2009; Pan et al. 2010) and studying the interaction energies (Day et al. 2000; Gordon et al. 2007) involved in the sorption processes at a molecular level. The kinetics can reveal the adsorption behavior over time, and the tendency of adsorbates to desorb from the adsorbent surface (Pan et al. 2010). Adsorption energy calculations at the optimum configuration of the adsorbent and adsorbate molecules suggest preferences for one molecule over the other for the same adsorbent. Extensive investigation of the adsorption characteristics (Bautista-Toledo et al. 2005; Feng et al. 2010; Liu et al. 2009) of EDCs on SWNTs is important not only to develop SWNTs as an EDC removal technology, but also to studying possible facilitated transport of EDCs (by SWNTs) co-existing with SWNTs in aqueous systems.

The objective of this paper is to perform a mechanistic study of the sorption behavior of BPA and E2 on both SWNTs and acid-treated SWNTs (t-SWNTs) using physicochemical characterization and molecular modeling. In this study, as-received SWNTs and t-SWNTs are used to compare the adsorption of two representative EDCs (i.e., BPA and E2). The adsorption energies of the SWNTs with BPA and E2 are calculated at the molecular level using Density Functional Theory (DFT). Sorption experiments are performed at different temperatures, and the results are analyzed using a pseudo-second-order kinetic model. The SWNTs are characterized in detail by transmission and high-resolution transmission electron microscopy (TEM and HRTEM), electrophoresis, static light scattering (SLS), and Raman spectroscopy.

2 Materials and Methods

2.1 Materials

BPA (purity>99%), E2 (purity>99%), sodium chloride, dibasic potassium phosphate, ammonium persulfate, sodium hydroxide (50% solution in water), and hydrochloric acid (37%) were obtained from Sigma Aldrich (St. Louis, MO, USA). Phosphoric acid (85% purity) was purchased from Fisher Scientific (Pittsburgh, PA, USA), and methanol (high-performance liquid chromatography (HPLC) grade) and sulfuric acid (96% purity) were obtained from Acros Organics (Morris Plains, NJ, USA). Deionized (DI) ultrapure water, having a resistivity greater than 18 mΩ, was used in all experiments. Dialysis membranes (molecular weight cutoffs, 12,000–14,000 g/mole) were supplied by Spectrum Laboratories (Rancho Dominguez, CA, USA). SWNTs were acquired from Cheap Tubes Inc. (Brattleboro, VT, USA).

2.2 Preparation of Acidified SWNTs

SWNTs were oxidized using ammonium persulfate and sulfuric acid by employing a previously developed experimental protocol (Moreno-Castilla et al. 1997). The nanomaterial to oxidant ratio used for the treatment was 1 g of SWNTs for every 100 mL of oxidizing solution. A saturated solution of ammonium persulfate was prepared by adding an excess amount of ammonium persulfate (~150 g) to 200 mL of 1 M H_2SO_4. After stirring for 48 h, the saturated ammonium persulfate solution was filtered using a 0.7-μm glass microfiber filter (Whatman GF/F) with a vacuum pump. The filtrate (saturated ammonium persulfate solution) was used to oxidize (treat) the SWNTs by refluxing for 24 h. An equal volume of water was added to the (treated) t-SWNTs to increase the pH of the suspension, thus decreasing the SWNT concentration by half (from 10 to 5 mg/mL). This suspension was then transferred to dialysis bags. Dialysis was carried out in DI ultrapure water in a continuous flow reactor until the pH of the DI ultrapure water leaving the reactor reached approximately 6.5 (Fig. S1). A suspension of t-SWNTs at a concentration of 5 mg/mL was achieved with an ambient pH of 6.5±0.5.

2.3 Characterization of SWNTs

The morphology and microstructure of the SWNTs and t-SWNTs were studied using a TEM (Hitachi H-8000, accelerating voltage 200 kV) fitted with an AMT side-mount charge-coupled device (CCD) camera, and a HRTEM (JEOL JEM 2100F, accelerating voltage 200 kV) fitted with a Schottky field emission gun, a Gatan UltraScan 2×2 k camera, and a Fischione HA-ADF detector. Samples were dispersed in DI ultrapure water using mild ultrasonication (1 kJ/10 mL) and deposited on a 200-mesh nickel or copper grid coated with formvar. (Gonzo and Gonzo 2005)

The zeta potential of the SWNTs was measured at a concentration of 1 mg/L with a ZetaPALS analyzer (Brookhaven, NY). The pH of the SWNT solutions was adjusted from 3.5 to 11.0 by adding 1 M HCl or 1 M NaOH solution. The zeta potential was calculated from the electrophoretic mobility (μ) values by using the Smoluchowski equation:

$$\mu = \frac{\zeta \in V}{4\pi\eta d} \tag{1}$$

where ζ is the zeta potential, ϵ is the dielectric constant of the medium (water in this case), V is the applied voltage, η is the viscosity of the suspension, and d is the electrode separation (Saleh et al. 2008; Saleh et al. 2010).

Raman spectra were collected using a LabRam JY Horiba Raman spectrometer fitted with a thermoelectrically cooled CCD, a confocal microscope, and a 632 nm He–Ne laser for excitation. Samples were prepared by dispersing SWNTs in DI ultrapure water and then drying them overnight on glass slides in a desiccator. The integration time was 15 s per scan; each spectrum represents an average of five scans (Saleh et al. 2008; Saleh et al. 2010).

SLS was examined using a precision dynamic/static light scattering (DLS/SLS) instrument. Scattering intensity data were obtained through an angular range of 30–90°. The fractal dimension (D_f) of the SWNT clusters was measured by plotting the scattering parameter (q) versus the intensity (I). The scattering parameter can be represented by

$$q = \frac{4\pi r}{\lambda_0} \sin\left(\frac{\theta}{2}\right) \tag{2}$$

where r is the refractive index of the solvent (i.e., water) and λ_0 is the wavelength of light.

2.4 Batch Adsorption Experiments

BPA and E2 were dissolved separately in methanol to produce stock solutions of 1 mM each. The stock solutions were diluted in DI ultrapure water to the desired concentrations (1 μM BPA and 1 μM E2). They were then mixed with the adsorbents (SWNTs/t-SWNTs) at room temperature (~23°C). Batch adsorption experiments were performed using 1 L glass beakers covered with aluminum foil to avoid contamination and maintain the system temperature. SWNTs/t-SWNTs (10 mg/L) and 1 μM each of BPA and E2 were added to the glass beakers, which were then placed on a hotplate stirrer (Isotemp) purchased from Fisher Scientific (Pittsburgh, PA). A constant angular speed of 200 rpm was maintained during the experiments, and temperatures of 280, 295, and 315 K were used depending on the experimental requirements. The temperature of the solution was measured continuously using a mercury thermometer. A pH of 7.5 was maintained by adding 1 M HCl or 1 M NaOH in the presence of a 1 mM phosphate buffer, and a conductivity of 300 μS/cm was obtained by using a 2 M NaCl solution.

2.5 Analytical Method

A HPLC system (HP1200 HPLC) was used to determine the concentrations of BPA and E2; the system included a quaternary pump (G1312A) and a fluorescence detector set at an excitation wavelength of 280 nm and an emission wavelength of 310 nm. An automated liquid sampler (G1329A; Agilent, Santa Clara, CA, USA) was also used. Data were collected and integrated using an Agilent Chemstation. The analytical column was a LiChrospher RP 18 with dimensions of 150 mm×4.6 mm and an internal diameter of 5 μm, manufactured by EMD Chemicals (Milford, MA, USA).The mobile-phase solvent profile was 45% DI ultrapure water acidified with 10 mM H_3PO_4 and 55% methanol, with a constant flow rate of 1 mL/min for 23 min per sample. The chromatographic analysis was performed at 30°C with a flow rate of 1.0 mL/min and an injection volume of 50 μL. BPA and E2 were eluted from the column at 9.6 and 21.2 min, respectively. The HPLC was calibrated whenever the samples containing BPA and E2 were analyzed. The method detection limit (MDL) for BPA and E2 was 0.01 μM. MDLs were determined for these compounds by reverse-phase HPLC with fluorescence detection by injecting 50 μL of a 0.05 μM of each of these compounds 8 times and reported with 99% confidence based upon the calculation of variance and standard deviation of the replicate measurements following United State Environmental Protection Agency MDL method (Revision 1.11).

2.6 Adsorption Energy Calculations

The general approach to calculating adsorption energies of the EDCs onto SWNTs and graphene was similar to that of Stepanian et al. (2009), who calculated the interaction energies of an adsorbate onto a SWNT cutout with fixed coordinates. Graphene was also simulated in this study to evaluate the possible interaction of EDCs with fragments of the SWNTs.

The initial geometry of a SWNT molecule with a chirality of (18,0) was obtained from VMD (Humphrey et al. 1996). The ends of the SWNT were terminated with H atoms, and the resulting molecular formula was $C_{288}H_{36}$. Graphene was initially obtained from a SWNT molecule with a chirality of (10,0) that was cut along the longitudinal axis. The carbon molecules along the edge were terminated with H atoms to obtain a molecular formula of $C_{252}H_{44}$, and the molecule was allowed to relax to a flat configuration during geometry optimization. The coordinates of the SWNT and graphene molecule were optimized (Kastner et al. 2009) by the DFT using the B3LYP5 functional and the 3–21G basis set, as implemented in TeraChem (Ufimtsev and Martinez 2009).

To evaluate the adsorption energy of the EDCs with the SWNTs and graphene, an estimate of the initial geometry was obtained by optimizing fragments of the molecules using their effective fragment potentials (EFP2), as generated using GAMESS (Gordon et al. 2005; Gordon et al. 2007; Schmidt et al. 1993; Smith et al. 2008). The optimized SWNT and graphene molecules were re-oriented to their principal axis configuration using MacMolPlt (Bode and Gordon 1998). A C_{54} fragment was cut from the center of the large molecules, and the external carbons were terminated with H atoms. The H positions were then optimized at the DFT/B3LYP5/3–21G level while keeping the C atoms fixed (Ufimtsev and Martinez 2009). The EFP2 were generated at the 6–31G level (Gordon et al.

2005; Schmidt et al. 1993). The EDCs were optimized at the MP2/6–31G(d) level, and their EFP was generated at the 6–31++G(d,p) level (Gordon et al. 2005; Schmidt et al. 1993). Geometry optimization of the fragments was performed by randomly rotating the EDCs and locating their center 1.5–10 angstroms (Å) perpendicular to the surface of the SWNT or graphene, with the initial nearest distance between the atoms limited to 1.5–5 Å. A total of 10,000 optimized configurations were collected, and the lowest energy configuration was selected for further geometry optimization.

The lowest energy configurations were mapped onto a larger $C_{96}H_{24}$ SWNT or graphene cutout, and geometry optimization was performed at the DFT/B3LYP5/6–31G level with dispersion corrections (Grimme et al. 2010; Grimme et al. 2011). The coordinates of the SWNT and graphene were kept fixed. The final energy was calculated at the DFT-D/B3LYP5/6–31++G(d,p) level, and the adsorption energy between the SWNT molecules and EDCs was calculated as:

$$\text{Adsorption energy} = \text{E(SWNT} + \text{EDC)} - \text{E(SWNT)} - \text{E(EDC)} \quad (3)$$

E(EDC) was calculated with its geometry optimized at the DFT-D/B3LYP5/6–31G level. Similar calculations were made for graphene.

3 Results and Discussion

3.1 Characterization of SWNTs and t-SWNTs

Figure 1 shows the purified SWNTs before and after acid treatment; these images are consistent with earlier observations (Chiang et al. 2001; Hu et al. 2003; Niyogi et al. 2002; Zhang et al. 2003). HRTEM images provide further evidence of the predominance of SWNTs (Fig. 1c). The average bundle width was determined to be approximately 20 nm from Fig. 1c.

Figure 2 shows the variation in zeta potential as a function of pH for SWNTs and t-SWNTs. Acid treatment enhances the negative surface potential on SWNT surfaces for the entire pH range (pH 3.5–10). The magnitude of surface potential increases from −21.4±2.7 mV (for SWNTs at pH 3.5) to −70.3± 4.8 mV (for t-SWNTs at pH 11.0). This increase in negative surface potential upon functionalization has been consistently reported in other studies (Chen et al. 2005; Hu et al. 2005; Kuo 2009; Saleh et al. 2010; Yu et al. 2009). However, the variability in surface charge enhancement as observed in the literature is thought to depend on the SWNT manufacturing processes (Hersam 2008) and/or mode of SWNT treatment. It has been proposed in the literature that an electrical double layer on the surface of SWNTs is responsible for their net charge on the helical carbon structures (Hu et al. 2005). This provides electrostatic repulsion between two

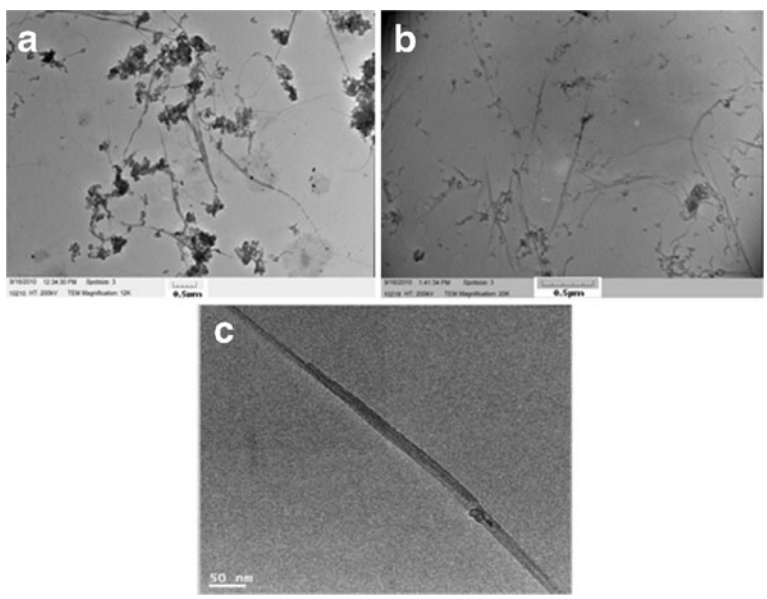

Fig. 1 TEM images of **a** SWNTs, **b** t-SWNTs, and **c** HRTEM image of SWNT bundle

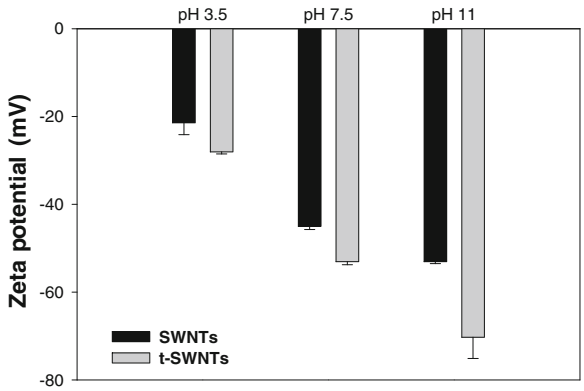

Fig. 2 Zeta potential of SWNTs at various pH conditions (SWNTs/t-SWNTs=1 mg/L and conductivity=600 μS/cm NaCl) in DI water. The measurements were performed at 22±1°C

SWNTs and is adequate to stabilize SWNT aqueous suspensions. The increase in pH (3.5 to 11) enhances the negative surface charge for both SWNTs (−21.4± 2.7 mV to −53.1±0.5 mV) and t-SWNTs (−28.1± 0.5 mV to −70.3±4.8 mV). Such enhancement in surface potential indicates pH-dependent deprotonation of dissociable functional groups (e.g., −COOH) that have most likely been incorporated on the surfaces of t-SWNTs through acid etching process (Hu et al. 2005). The higher surface potential on t-SWNTs compared to untreated SWNTs indicates enhanced colloidal stability for the t-SWNTs as confirmed by light scattering measurements.

Raman spectroscopy is widely used to characterize carbon nanotubes (Dresselhaus et al. 2002; Gruneis et al. 2002; Jorio et al. 2001; Ma et al. 2009; Saleh et al. 2008; Saleh et al. 2010). Low-frequency micro-Raman spectra of SWNTs and t-SWNTs are shown in Fig. 3a; these spectra exhibit the characteristic radial breathing mode (RBM) and peaks in the D and G band regions. The peak frequencies for the SWNTs and t-SWNTs are 214 and 212 cm^{-1}, respectively, in the RBM region. Such peak behavior can be used to estimate the SWNT diameters using the following correlation (Ma et al. 2009):

$$d = \frac{223.14}{\omega - 14} \tag{4}$$

where ω is the Raman shift and d is the SWNT diameter. On the basis of the observed peaks, the diameters of SWNTs and t-SWNTs are estimated to be 1.10 (ω=214 cm^{-1}) and 1.13 nm (ω=212 cm^{-1}), respectively (Costa and Borowiak-Palen 2009; Kukovecz et al. 2003). This slight increase in the diameter of the SWNTs following acid treatment can be explained by exohedral functionalization (Costa and Borowiak-Palen 2009). Defects on the SWNTs become active sites for carboxylic and hydroxyl group formation, which interact with the carbon in SWNTs, contracting the C–C bonds in their structure. Consequently, a shift occurs in the RBM corresponding to wider SWNTs. Figure 3b shows a second group of Raman peaks appearing at 1,345 (D band) and 1,585 cm^{-1} (G band). The D band response is induced by defect features on the SWNT surfaces and edges, including the presence of minor amorphous carbon and hollow graphite particles in the sample. The strong intensity of the G band is related to the E_{2g} graphite mode, and represents proper graphitization of carbon nanotubes (Dresselhaus et al. 2002; Gruneis et al. 2002; Souza Filho et al. 2003). The intensity ratio of the D to G peaks (I_D/I_G) is an indicator of the presence of carbon nanotube defects. I_D/I_G increases from 0.094 (SWNTs) to 0.120 (t-SWNTs) after acid etching. Such increase in defect sites were likely to have been induced by tube breakage and shortening upon acidification (Chen et al. 2005; Costa and Borowiak-Palen 2009; Dresselhaus et al. 2002; Saleh et al. 2010).

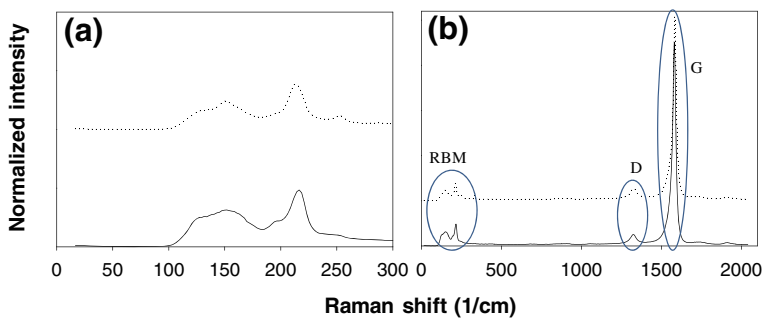

Fig. 3 Raman spectra of SWNTs (*solid line*) and t-SWNTs (*dotted line*) at (**a**) low and (**b**) high frequencies

SLS can help clarify the morphology of SWNT aggregates. Figure 4 illustrates the decrease in scattering intensity (I) with wave factor (q) used to estimate the fractal dimension (D_f) of SWNTs and t-SWNTs, which is useful for evaluating the compactness of aggregates. Forrest and Witten (1979) were the first to explain the fractal nature of particle aggregates. They were limited to studying three-dimensional metallic oxide smoke particles by depositing them onto a two-dimensional TEM substrate. This limitation caused them to record incorrect measurements. A number of researchers later addressed the problem (Burns et al. 1997). In our studies, D_f increases from 2.66 to 2.81 upon treatment of the SWNTs. This shows that t-SWNT aggregates are considerably more compact than SWNT aggregates, which may be due to the increase in the diameter of SWNTs with the addition of functional groups during acid treatment (Costa and Borowiak-Palen 2009). Another explanation for the greater compactness is the proper stacking of t-SWNTs due to the absence of impurities, including metal catalyst particles (Fig. 1) and/or debris (Chiang et al. 2001). It might also be possible that the electrostatic repulsion provided by the higher density functional groups on the t-SWNTs allowed for sustained stability and therefore better packing of the treated SWNTs. Such compactness must have reduced the interstitial spaces and groove areas in the SWNT aggregates. Agnihoteri et al. (Agnihotri et al. 2005) described four adsorption sites on SWNTs: (a) inside the tubes, (b) interstitial channels, (c) external groove areas, and (d) external surfaces of aggregates. A previous study has suggested that the groove areas and interstitial spaces were the most suitable places to accommodate butterfly-shaped BPA molecules (Pan et al. 2008). As stated above, the compactness of the SWNT bundle ultimately eliminates the groove areas and interstitial spaces, and therefore BPA adsorption is expected to be significantly reduced by acid treatment of SWNTs.

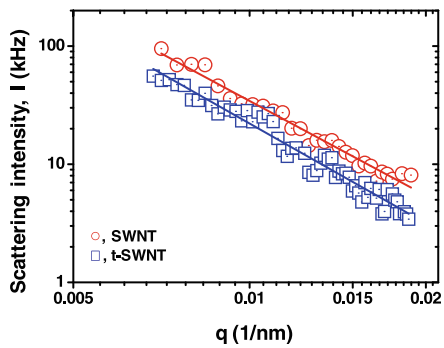

Fig. 4 Angle-dependent (30°–85°) static light scattering profile of q vs I for SWNTs and t-SWNTs in fractal regime. The measurements were performed at 22±1°C

3.2 Adsorption and Kinetics

Figure 5 illustrates the adsorption of BPA and E2 to SWNTs and t-SWNTs at varied temperatures over an

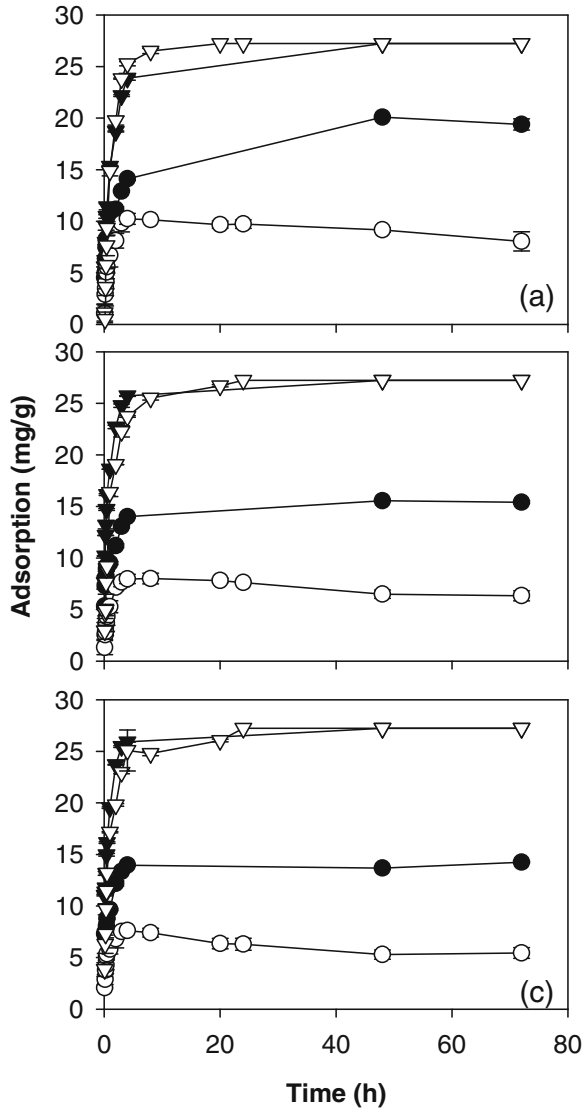

Fig. 5 Adsorption onto SWNTs (*filled circle*) and t-SWNTs (*circle*) for BPA and onto SWNTs (*filled inverted triangle*) and t-SWNTs (*inverted triangle*) for E2 at **a** 280 K, **b** 295 K, and **c** 315 K (Co=1 μM; pH=7.5; conductivity 300=μS/cm NaCl)

equilibration period of 72 h. A total of 19.4, 15.4, and 14.3 mg/g of BPA were adsorbed on SWNTs, while a total of 8.0, 6.4, and 5.1 mg/g were adsorbed on t-SWNTs at 280, 295, and 315 K, respectively. Equilibrium concentrations of BPA and E2 appear to be achieved after approximately 4 h, which is consistent with the rapid equilibrium times observed in previous studies (Joseph et al. 2011; Lu et al. 2005). This decrease in BPA sorption with increasing temperature can be attributed to the associated exothermic reaction mechanism elaborated elsewhere (Feng et al. 2010). At least 75% of the BPA was adsorbed on SWNTs in the first 4 h of contact.

The equilibrium adsorption capacity of SWNTs for BPA decreases with increasing temperature (Fig. 5), but is consistently higher than that of t-SWNTs. This behavior is similar to the sorption of aromatics on carbonaceous materials, which is dominated by the π–π interaction between the aromatic ring electrons in the adsorbate and those in the carbon nanotubes' basal planes (Coughlin and Ezra 1968). The acidification of SWNTs decreases their adsorption capacity for BPA by introducing carboxyl groups on the surfaces of the tubes. This occurs because the carboxyl groups evoke electron deficiencies by withdrawing electrons from the graphitic nanotube layers, resulting in high electronegativity at the functional group ends. Such electronegative functional groups enhance hydrogen bond formation and thereby increase affinity of water to t-SWNTs (Liu et al. 2009). Therefore, the possible clustering of water molecule on the surface of t-SWNTs inhibits BPA adsorption. The amount of BPA adsorption depends largely on the presence of acidic oxygen-containing groups and the surface charge density of SWNTs. Furthermore, the decrease in sorption of BPA to t-SWNTs can further be supported by reduced interstitial spaces as demonstrated by increased D^f upon functionalization (Fig. 4 and SWNT/t-SWNT characterization section discussion).

Adsorption of E2 is thought to be irreversible, because all the E2 in the aqueous solution remained sorbed during the studied time period of 72 h (Yoon et al. 2003). Also, no significant difference between the adsorption capacity of SWNTs and t-SWNTs for E2 was observed. Overall, a significantly larger fraction of E2 was removed by both SWNTs and t-SWNTs, as compared to BPA. The larger removal of E2 over BPA can presumably be explained by the differences in logarithmic octanol-water partition coefficients of these molecules (log Kow; 3.9 for E2 and 3.3 for BPA) (Yoon et al. 2003). This suggests that non-specific interactions between the sorbate molecules and the sorbent SWNT/t-SWNT surfaces, e.g., hydrophobic interactions (i.e., adsorption), are one of the dominant mechanisms. Several previous studies using

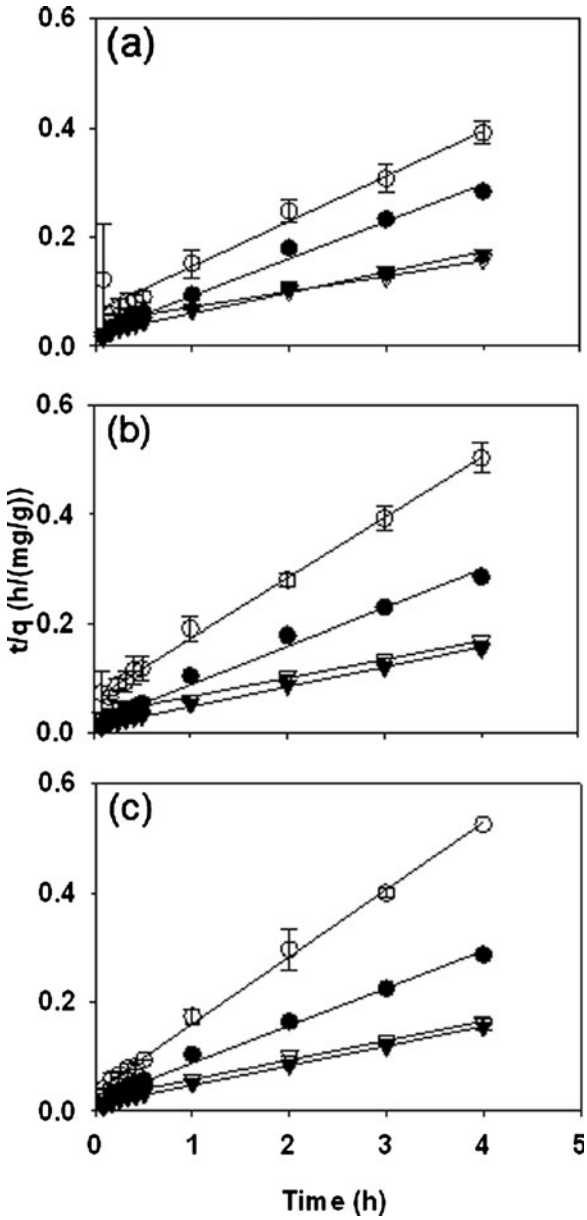

Fig. 6 Adsorption onto SWNTs (*filled circle*) and t-SWNTs (*circle*) for BPA and onto SWNTs (*filled inverted triangle*) and t-SWNTs (*inverted triangle*) for E2 fitted by pseudo second-order kinetic equation at **a** 280 K, **b** 295 K, and **c** 315 K (Co= 1 μM; pH=7.5; conductivity 300=μS/cm NaCl)

SWNTs as sorbents, describe hydrophobic interaction as a key mechanism where CNT surfaces are mentioned "evenly distributed hydrophobic sites" for organic compound adsorption (Gotovac et al. 2007; Pan et al. 2008). In addition, as described earlier, the π–π electron donor–acceptor interactions may be an additional mechanism for the adsorption of BPA and E2. Such large differences between E2 and BPA sorption can be mechanistically studied at molecular interaction level as described in the next section.

A pseudo-second-order kinetic model was adopted in order to elucidate the kinetics of the adsorption process. The pseudo-second-order model is expressed as (Blanchard et al. 1984):

$$\frac{t}{q} = \frac{1}{k_2 q_e^2} + \frac{t}{q_e} \tag{5}$$

where q_e and q are defined as in the pseudo-first-order kinetic model, and k_2 (g/mg-h) is the rate constant of the pseudo-second-order model for adsorption. k_2 can be estimated from the intercept of a linear plot of t/q versus time t. Figure 6 shows the calculated adsorption kinetics of BPA and E2 on SWNTs and t-SWNTs, using data from a 4-h contact time. The data were fitted by the pseudo-second-order kinetic model. Currently, first- and second-order models are frequently applied to describe the adsorption of organic chemicals onto SWNTs (Feng et al. 2010; Hu et al. 2009; Upadhyayula et al. 2009). The suitability of the kinetic model was determined by calculating the correlation coefficient (R^2). The adsorption kinetic constants are listed in Table 1. Overall, the pseudo-second-order model fits both the SWNT and t-SWNT sorption data well, as verified by the R^2 values (≅0.99). This is consistent with a previous study, which stated that the pseudo-second-order kinetic model was better suited for describing the adsorption behaviors of BPA for untreated adsorbents (Liu et al. 2009).

3.3 Adsorption Energy

While the hydrophobic interactions and π–π electron donor–acceptor interactions are the widely two known mechanisms for organic compound adsorption on SWNTs, determining the adsorption energy of the EDCs with the SWNTs and graphene is important to understand EDC removal by the adsorbents. Figure 7 shows SWNT and graphene configurations used in the final geometry optimization, as well as the lowest energy configurations and interaction energies of the EDCs adsorbed onto the SWNT and graphene. The lowest energy configuration of the E2 occurs when the methyl group is oriented away from the surface of the SWNT and graphene, which allows for the maximum overlap of orbitals between E2 and the adsorbent. The phenol rings of the BPA are equally oriented at an angle to the graphene to maximize π–π interactions. On the SWNT, one phenol ring of the BPA is oriented nearly parallel to the curved surface, while the other ring

Table 1 Summary of BPA and E2 adsorption data evaluated by second order kinetic model

Compound	Temperature	SWNTs/t-SWNTs	$q_{e,\,exp}$[a] (mg/g)	$q_{e,\,cal}$[b] (mg/g)	k_2 (g/mg-h)	R^2
BPA	280 K	SWNTs	18.2	14.6	0.13	0.99
	295 K		14.6	14.3	0.25	0.99
	315 K		13.7	14.6	0.28	0.99
	280 K	t-SWNTs	9.53	12.1	0.18	0.96
	295 K		7.42	9.05	0.30	0.99
	315 K		6.53	8.12	0.64	0.99
E2	280 K	SWNTs	25.5	26.5	0.07	0.99
	295 K		26.6	27.5	0.11	0.99
	315 K		26.7	27. 8	0.12	0.99
	280 K	t-SWNTs	26.9	35.2	0.03	0.99
	295 K		26.2	29.3	0.04	0.99
	315 K		26.2	28.1	0.06	0.99

[a] Experimental data

[b] Calculated data from model

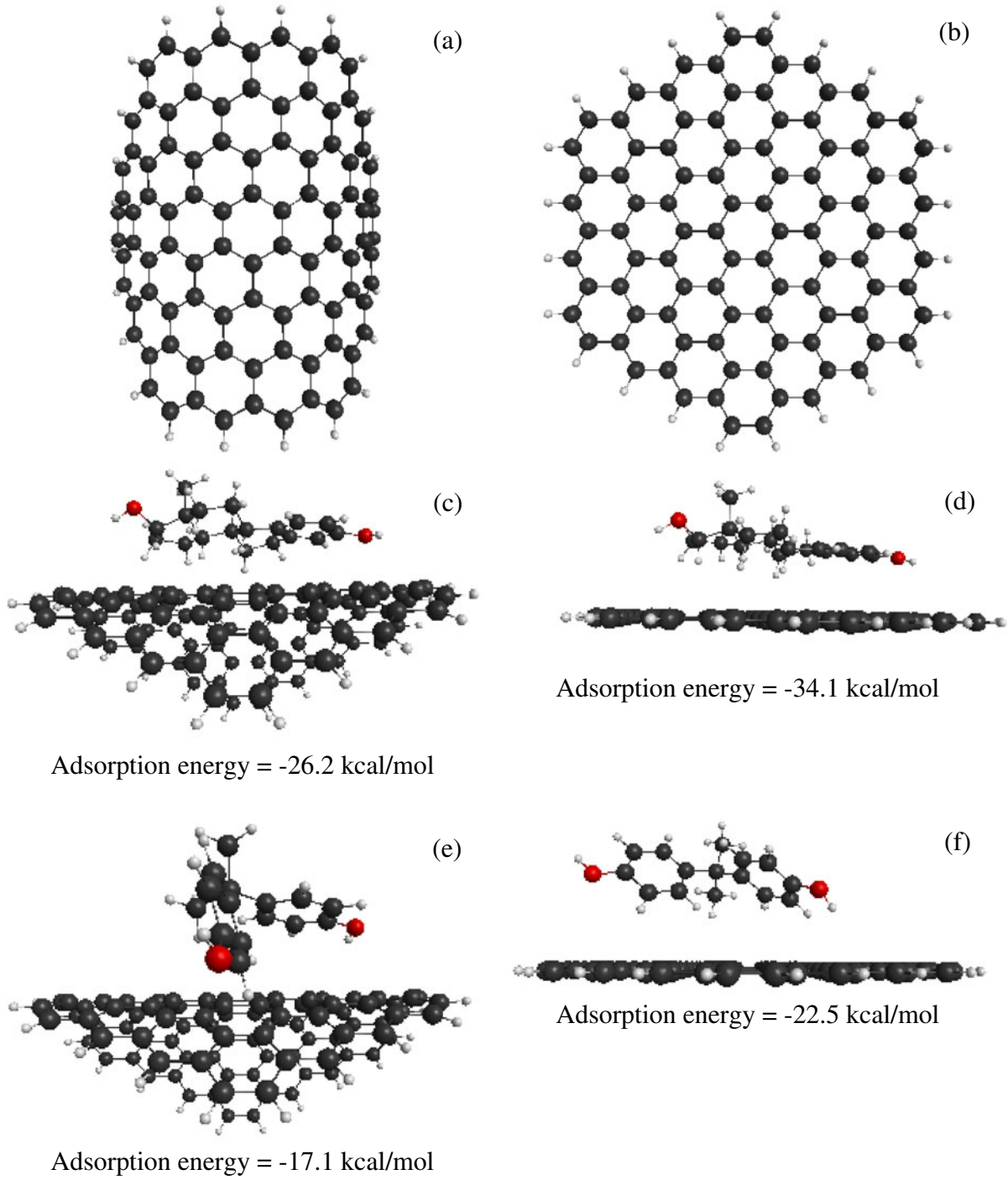

Fig. 7 **a** SWNT and **b** graphene molecular models used in this study. Energy minimized configuration and adsorption energies of **c** E2 on SWNT, **d** E2 on graphene, **e** BPA on SWNT, and **f** BPA on graphene

is almost perpendicular. In all cases, E2 (−26.2 kcal/mol on SWNT and −34.1 kcal/mol on graphene) has a more negative and favorable adsorption energy than BPA (−17.1 kcal/mol on SWNT and −22.5 kcal/mol on graphene), because E2 is a larger molecule, which allows for more overlap of the adsorbate orbitals with the

adsorbent. These results are consistent with experimental observations of significantly lower sorption of BPA compared to E2. Adsorption on graphene is more favorable than on SWNTs, because the absence of curvature on the graphene molecule allows for a larger overlap with the EDC orbitals. This is consistent with a previous study that shows an increase in interaction energy with nanotube diameter (Tournus and Charlier 2005).

4 Conclusions

The adsorption of BPA and E2 onto SWNTs and t-SWNTs was investigated at various temperatures. Several analytical techniques, including TEM, zeta potential measurements, and Raman spectra, confirmed the acidification of SWNTs. SWNTs and t-SWNTs were successfully employed to adsorb BPA and E2. The equilibrium adsorption capacity of SWNT for BPA decreased with increasing temperature, while it was consistently higher than that of t-SWNTs. However, E2 adsorption remained high with the varying temperature. The experimental data for sorption, fitted well with the pseudo-second-order kinetic model. A significantly larger fraction of E2 was removed by both SWNTs and t-SWNTs, as compared to BPA. The higher adsorption of E2 can be explained by its high hydrophobicity, suggesting that hydrophobic adsorption of the EDCs by the SWNTs and t-SWNTs was the dominant removal mechanism. Furthermore, the DFT calculations provided with unique insight onto the molecular structure of the two chemicals and their interaction with graphitic sorbent structures. Such adsorption energy calculations confirmed the preferential sorption of E2 compared to BPA by both SWNTs and t-SWNTs, and demonstrated that optimized geometric orientation of the molecules dominated their π–π interactions and thereby their sorption behavior. The preference for E2 over BPA for adsorption on a layer of carbon atoms was explained well by the adsorption energy calculations. Such molecular-level analysis is rarely performed for typical environmental sorption studies. This study has demonstrated the importance of such mechanistic analysis, which can successfully decipher sorption mechanisms and provide valuable insight into EDC removal processes.

Acknowledgments This research was supported by GS E&C and the Korea Ministry of Environment, "Project, 414-111-004." The authors also acknowledge the University of South Carolina's High Performance Computing Group for the computing time used in this research.

References

Agnihotri, S., Mota, J. P. B., Rostam-Abadi, M., & Rood, M. J. (2005). Structural characterization of single-walled carbon nanotube bundles by experiment and molecular simulation. *Langmuir, 21*, 896–904.

Baughman, R. H., Zakhidov, A. A., & de Heer, W. A. (2002). Carbon nanotubes: the route toward applications. *Science, 297*, 787–792.

Bautista-Toledo, I., Ferro-García, M. A., Rivera-Utrilla, J., Moreno-Castilla, C., & Vegas Fernández, F. J. (2005). Bisphenol A removal from water by activated carbon: effects of carbon characteristics and solution chemistry. *Environmental Science & Technology, 39*, 6246–6250.

Blanchard, G., Maunaye, M., & Martin, G. (1984). Removal of heavy metals from waters by means of natural zeolites. *Water Research, 18*, 1501–1507.

Bode, B. M., & Gordon, M. S. (1998). MacMolPlt: a graphical user interface for GAMESS. *Journal of Molecular Graphics & Modelling, 16*, 133–138.

Burns, J. L., Y-d, Y., Jameson, G. J., & Biggs, S. (1997). A light scattering study of the fractal aggregation behavior of a model colloidal system. *Langmuir, 13*, 6413–6420.

Chen, S., Shen, W., Wu, G., Chen, D., & Jiang, M. (2005). A new approach to the functionalization of single-walled carbon nanotubes with both alkyl and carboxyl groups. *Chemical Physics Letters, 402*, 312–317.

Chiang, I. W., Brinson, B. E., Smalley, R. E., Margrave, J. L., & Hauge, R. H. (2001). Purification and characterization of single-wall carbon nanotubes. *The Journal of Physical Chemistry. B, 105*, 1157–1161.

Costa, S., & Borowiak-Palen, E. (2009). Diameter sensitive effect in singlewalled carbon nanotubes upon acid treatment. *Journal of Alloys and Compounds, 486*, 386–390.

Coughlin, R. W., & Ezra, F. S. (1968). Role of surface acidity in the adsorption of organic pollutants on the surface of carbon. *Environmental Science & Technology, 2*, 291–297.

Day, P. N., Pachter, R., Gordon, M. S., & Merrill, G. N. (2000). A study of water clusters using the effective fragment potential and Monte Carlo simulated annealing. *The Journal of Chemical Physics, 112*, 2063–2073.

Dresselhaus, M. S., Dresselhaus, G., Jorio, A., Souza Filho, A. G., & Saito, R. (2002). Raman spectroscopy on isolated single wall carbon nanotubes. *Carbon, 40*, 2043–2061.

Fan, Z., Casey, F. X. M., Hakk, H., & Larsen, G. L. (2007). Persistence and fate of 17β-estradiol and testosterone in agricultural soils. *Chemosphere, 67*, 886–895.

Feng, Y., Zhang, Z., Gao, P., Su, H., Yu, Y., & Ren, N. (2010). Adsorption behavior of EE2 (17α-ethinylestradiol) onto the inactivated sewage sludge: Kinetics, thermodynamics and influence factors. *Journal of Hazardous Materials, 175*, 970–976.

Ferguson, P. L., Chandler, G. T., Templeton, R. C., DeMarco, A., Scrivens, W. A., & Englehart, B. A.

(2008). Influence of sediment-amendment with single-walled carbon nanotubes and diesel soot on bioaccumulation of hydrophobic organic contaminants by benthic invertebrates. *Environmental Science & Technology, 42*, 3879–3885.

Forrest, S. R., & Witten, T. A., Jr. (1979). Long-range correlations in smoke-particle aggregates. *Journal of Physics A: Mathematical and General, 12*, L109.

Furtado, C. A., Kim, U. J., Gutierrez, H. R., Pan, L., Dickey, E. C., & Eklund, P. C. (2004). Debundling and dissolution of single-walled carbon nanotubes in amide solvents. *Journal of the American Chemical Society, 126*, 6095–6105.

Gonzo, E., & Gonzo, L. (2005). Kinetics of phenol removal from aqueous solution by adsorption onto peanut shell acid-activated carbon. *Adsorption Science and Technology, 23*, 289–302.

Goodson, A., Robin, H., Summerfield, W., & Cooper, I. (2004). Migration of bisphenol A from can coatings—effects of damage, storage conditions and heating. *Food Additives and Contaminants, 21*, 1015–1026.

Gordon, M.S., Schmidt, M.W., Dykstra, C.E., Frenking, G., Kim, K.S., Scuseria, G.E. (2005). Advances in electronic structure theory: GAMESS a decade later. Theory and applications of computational chemistry: the first forty years. Elsevier, p 1167–1189.

Gordon, M.S., Slipchenko, L., Li, H., Jensen, J.H., Spellmeyer, D.C., Wheeler, R. (2007). The effective fragment potential: a general method for predicting intermolecular interactions. Annual reports in computational chemistry. Elsevier, p 177–193.

Gotovac, S., Yang, C. M., Hattori, Y., Takahashi, K., Kanoh, H., & Kaneko, K. (2007). Adsorption of polyaromatic hydrocarbons on single wall carbon nanotubes of different functionalities and diameters. *Journal of Colloid and Interface Science, 314*, 18–24.

Grimme, S., Antony, J., Ehrlich, S., & Krieg, H. (2010). A consistent and accurate ab initio parametrization of density functional dispersion correction (DFT-D) for the 94 elements H-Pu. *Journal of Chemical Physics, 132*, 154104.

Grimme, S., Ehrlich, S., & Goerigk, L. (2011). Effect of the damping function in dispersion corrected density functional theory. *Journal of Computational Chemistry, 32*, 1456–1465.

Gruneis, A., Saito, R., Kimura, T., Cançado, L. G., Pimenta, M. A., Jorio, A., Souza, A. G., Dresselhaus, G., & Dresselhaus, M. S. (2002). Determination of two-dimensional phonon dispersion relation of graphite by Raman spectroscopy. *Physical Review B, 65*, 155405.

Hersam, M. C. (2008). Progress towards monodisperse single-walled carbon nanotubes. *National Nanotechnology, 3*, 387–394.

Ho, Y. S., Ng, J. C. Y., & McKay, G. (2000). Kinetics of pollution sorption by biosorbents. *Review in Separation and Purification Methods, 29*, 189–232.

Hu, H., Zhao, B., Itkis, M. E., & Haddon, R. C. (2003). Nitric acid purification of single-walled carbon nanotubes. *The Journal of Physical Chemistry. B, 107*, 13838–13842.

Hu, H., Yu, A., Kim, E., Zhao, B., Itkis, M. E., Bekyarova, E., & Haddon, R. C. (2005). Influence of the zeta potential on the dispersability and purification of single-walled carbon nanotubes. *The Journal of Physical Chemistry. B, 109*, 11520–11524.

Hu, J., Chen, C. L., Zhu, X. X., & Wang, X. K. (2009). Removal of chromium from aqueous solution by using oxidized multiwalled carbon nanotubes. *Journal of Hazardous Materials, 162*, 1542–1550.

Huang, Q., & Weber, W. J. (2005). Transformation and removal of bisphenol A from aqueous phase via peroxidase-mediated oxidative coupling reactions: efficacy, products, and pathways. *Environmental Science & Technology, 39*, 6029–6036.

Humphrey, W., Dalke, A., & Schulten, K. (1996). VMD: visual molecular dynamics. *Journal of Molecular Graphics, 14*, 33–38.

Jorio, A., Saito, R., Hafner, J. H., Lieber, C. M., Hunter, M., McClure, T., Dresselhaus, G., & Dresselhaus, M. S. (2001). Structural (n, m) determination of isolated single-wall carbon nanotubes by resonant Raman Scattering. *Physical Review Letters, 86*, 1118.

Joseph, L., Zaib, Q., Khan, I. A., Berge, N. D., Park, Y. G., Saleh, N. B., & Yoon, Y. (2011). Removal of bisphenol A and 17a-ethinyl estradiol from landfill leachate using single-walled carbon nanotubes. *Water Research, 45*, 4056–4068.

Kastner, J., Carr, J. M., Keal, T. W., Thiel, W., Wander, A., & Sherwood, P. (2009). DL-FIND: an open-source geometry optimizer for atomistic simulations. *Journal of Physical Chemistry A, 113*, 11856–11865.

Kolpin, D. W., Furlong, E. T., Meyer, M. T., Thurman, E. M., Zaugg, S. D., Barber, L. B., & Buxton, H. T. (2002). Pharmaceuticals, hormones, and other organic wastewater contaminants in U.S. streams, 1999–2000: a national reconnaissance. *Environmental Science & Technology, 36*, 1202–1211.

Kukovecz, A., Pichler, T., Pfeiffer, R., Kramberger, C., & Kuzmany, H. (2003). Diameter selective doping of single wall carbon nanotubes. *Physical Chemistry Chemical Physics, 5*, 582–587.

Kuo, C. Y. (2009). Comparison with as-grown and microwave modified carbon nanotubes to removal aqueous bisphenol A. *Desalination, 249*, 976–982.

Laganà, A., Bacaloni, A., De Leva, I., Faberi, A., Fago, G., & Marino, A. (2004). Analytical methodologies for determining the occurrence of endocrine disrupting chemicals in sewage treatment plants and natural waters. *Analytica Chimica Acta, 501*, 79–88.

Li, Y.-H., Wang, S., Wei, J., Zhang, X., Xu, C., Luan, Z., Wu, D., & Wei, B. (2002). Lead adsorption on carbon nanotubes. *Chemical Physics Letters, 357*, 263–266.

Li, Y.-H., Wang, S., Zhang, X., Wei, J., Xu, C., Luan, Z., & Wu, D. (2003). Adsorption of fluoride from water by aligned carbon nanotubes. *Materials Research Bulletin, 38*, 469–476.

Liu, G., Ma, J., Li, X., & Qin, Q. (2009). Adsorption of bisphenol A from aqueous solution onto activated carbons with different modification treatments. *Journal of Hazardous Materials, 164*, 1275–1280.

Lu, C. S., Chung, Y. L., & Chang, K. F. (2005). Adsorption of trihalomethanes from water with carbon nanotubes. *Water Research, 39*, 1183–1189.

Ma, J., Wang, J. N., & Wang, X. X. (2009). Large-diameter and water-dispersible single-walled carbon nanotubes: synthesis, characterization and applications. *Journal of Materials Chemistry, 19*, 3033–3041.

Mauter, M. S., & Elimelech, M. (2008). Environmental applications of carbon-based nanomaterials. *Environmental Science & Technology, 42*, 5843–5859.

Moreno-Castilla, C., Carrasco-Marín, F., & Mueden, A. (1997). The creation of acid carbon surfaces by treatment with $(NH_4)_2S_2O_8$. *Carbon, 35*, 1619–1626.

Niyogi, S., Hamon, M. A., Hu, H., Zhao, B., Bhowmik, P., Sen, R., Itkis, M. E., & Haddon, R. C. (2002). Chemistry of single-walled carbon nanotubes. *Accounts of Chemical Research, 35*, 1105–1113.

Pan, B., & Xing, B. (2010). Competitive and complementary adsorption of bisphenol A and 17α-ethinyl estradiol on carbon nanomaterials. *Journal of Agricultural and Food Chemistry, 58*, 8338–8343.

Pan, B., Lin, D., Mashayekhi, H., & Xing, B. (2008). Adsorption and hysteresis of bisphenol A and 17α-ethinyl estradiol on carbon nanomaterials. *Environmental Science & Technology, 42*, 5480–5485.

Pan, B., Sun, K., & Xing, B. (2010). Adsorption kinetics of 17α-ethinyl estradiol and bisphenol A on carbon nanomaterials. II. Concentration-dependence. *Journal of Soils and Sediments, 10*, 845–854.

Plata, D. L., Gschwend, P. M., & Reddy, C. M. (2008). Industrially synthesized single-walled carbon nanotubes: compositional data for users, environmental risk assessments, and source apportionment. *Nanotechnology, 19*, 185706.

Pyrzynska, K., Stafiej, A., & Biesaga, M. (2007). Sorption behavior of acidic herbicides on carbon nanotubes. *Mikrochimica Acta, 159*, 293–298.

Saleh, N. B., Pfefferle, L. D., & Elimelech, M. (2008). Aggregation kinetics of multiwalled carbon nanotubes in aquatic systems: Measurements and environmental implications. *Environmental Science & Technology, 42*, 7963–7969.

Saleh, N. B., Pfefferle, L. D., & Elimelech, M. (2010). Influence of biomacromolecules and humic acid on the aggregation kinetics of single-walled carbon nanotubes. *Environmental Science & Technology, 44*, 2412–2418.

Schmidt, M. W., Baldridge, K. K., Boatz, J. A., Elbert, S. T., Gordon, M. S., Jensen, J. H., Koseki, S., Matsunaga, N., Nguyen, K. A., & Su, S. (1993). General atomic and molecular electronic structure system. *Journal of Computational Chemistry, 14*, 1347–1363.

Smith, T., Slipchenko, L. V., & Gordon, M. S. (2008). Modeling pi–pi interactions with the effective fragment potential method: the benzene dimer and substituents. *Journal of Physical Chemistry A, 112*, 5286–5294.

Snyder, S. A., Westerhoff, P., Yoon, Y., & Sedlak, D. L. (2003). Pharmaceuticals, personal care products, and endocrine disruptors in water: implications for the water industry. *Environmental Engineering Science, 20*, 449–469.

Souza Filho, A. G., Jorio, A., Samsonidze, G. G., Dresselhaus, G., Pimenta, M. A., Dresselhaus, M. S., Swan, A. K., & Uuml, S. M. (2003). Competing spring constant versus double resonance effects on the properties of dispersive modes in isolated single-wall carbon nanotubes. *Physical Review B, 67*, 035427.

Stepanian, S. G., Karachevtsev, M. V., Glamazda, V. A., & Adamowicz, L. (2009). Raman spectroscopy study and first-principles calculations of the interaction between nucleic acid bases and carbon nanotubes. *Journal of Physical Chemistry A, 113*, 3621–3629.

Su, F. S., & Lu, C. S. (2007). Adsorption kinetics, thermodynamics and desorption of natural dissolved organic matter by multiwalled carbon nanotubes. *Journal of Environmental Science and Health, 42*, 1543–1552.

Tournus, F., & Charlier, J. C. (2005). Ab initio study of benzene adsorption on carbon nanotubes. *Physical Review B, 71*, 165421.

Ufimtsev, I. S., & Martinez, T. J. (2009). Quantum chemistry on graphical processing units. 3. Analytical energy gradients, geometry optimization, and first principles molecular dynamics. *Journal of Chemical Theory and Computation, 5*, 2619–2628.

Upadhyayula, V. K. K., Deng, S. G., Smith, G. B., & Mitchell, M. C. (2009). Adsorption of Bacillus subtilis on single-walled carbon nanotube aggregates, activated carbon and NanoCeram (TM). *Water Research, 43*, 148–156.

Wang, F., Yao, J., Sun, K., & Xing, B. (2010). Adsorption of dialkyl phthalate esters on carbon nanotubes. *Environmental Science & Technology, 44*, 6985–6991.

Yang, K., & Xing, B. (2007). Desorption of polycyclic aromatic hydrocarbons from carbon nanomaterials in water. *Environmental Pollution, 145*, 529–537.

Yang, K., Zhu, L., & Xing, B. (2006). Adsorption of polycyclic aromatic hydrocarbons by carbon nanomaterials. *Environmental Science & Technology, 40*, 1855–1861.

Yoon, Y. M., Westerhoff, P., Snyder, S. A., & Esparza, M. (2003). HPLC-fluorescence detection and adsorption of bisphenol A, 17 beta-estradiol, and 17 alpha-ethynyl estradiol on powdered activated carbon. *Water Research, 37*, 3530–3537.

Yoon, Y., Ryu, J., Oh, J., Choi, B.-G., & Snyder, S. A. (2010). Occurrence of endocrine disrupting compounds, pharmaceuticals, and personal care products in the Han River (Seoul, South Korea). *Science of the Total Environment, 408*, 636–643.

Yu, A., Su, C.-C. L., Roes, I., Fan, B., & Haddon, R. C. (2009). Gram-scale preparation of surfactant-free, carboxylic acid groups functionalized, individual single-walled carbon nanotubes in aqueous solution. *Langmuir, 26*, 1221–1225.

Zhang, J., Zou, H., Qing, Q., Yang, Y., Li, Q., Liu, Z., Guo, X., & Du, Z. (2003). Effect of chemical oxidation on the structure of single-walled carbon nanotubes. *The Journal of Physical Chemistry. B, 107*, 3712–3718.